SOURCE DATA   TRANSPARENT PROCESS   OPEN ACCESS

THE EMBO JOURNAL

Cold-induced calreticulin OsCRT3 conformational changes promote OsCIPK7 binding and temperature sensing in rice

Xiaoyu Guo[1,2,†] (iD), Dajian Zhang[1,2,†] (iD), Zhongliang Wang[1,2], Shujuan Xu[1,2] (iD), Oliver Batistič[3], Leonie Steinhorst[3] (iD), Hao Li[4], Yuxiang Weng[4], Dongtao Ren[5], Jörg Kudla[3] (iD), Yunyuan Xu[1,6] (iD) & Kang Chong[1,2,6,*] (iD)

Abstract

Unusually low temperatures caused by global climate change adversely affect rice production. Sensing cold to trigger signal network is a key base for improvement of chilling tolerance trait. Here, we report that *Oryza sativa* Calreticulin 3 (OsCRT3) localized at the endoplasmic reticulum (ER) exhibits conformational changes under cold stress, thereby enhancing its interaction with CBL-interacting protein kinase 7 (OsCIPK7) to sense cold. Phenotypic analyses of *OsCRT3* knock-out mutants and transgenic overexpression lines demonstrate that OsCRT3 is a positive regulator in chilling tolerance. OsCRT3 localizes at the ER and mediates increases in cytosolic calcium levels under cold stress. Notably, cold stress triggers secondary structural changes of OsCRT3 and enhances its binding affinity with OsCIPK7, which finally boosts its kinase activity. Moreover, Calcineurin B-like protein 7 (OsCBL7) and OsCBL8 interact with OsCIPK7 specifically on the plasma membrane. Taken together, our results thus identify a cold-sensing mechanism that simultaneously conveys cold-induced protein conformational change, enhances kinase activity, and Ca^{2+} signal generation to facilitate chilling tolerance in rice.

Introduction

Rice originates from temperate climate zones and is sensitive to chilling stress, which imperils agricultural production worldwide (Zhu, 2016; Zhang *et al*, 2019b). It is vital to breed stress-tolerant cultivars that can withstand the increasing erratic temperatures caused by global climate change. Based on the different temperature ranges and physiological responses involved, cold stress can be classified as freezing stress (below 0°C) or chilling stress (0–20°C) (Guo *et al*, 2018). Understanding the mechanisms that regulate chilling tolerance will aid molecular breeding efforts to improve the cold-tolerance traits of rice.

Calcium (Ca^{2+}) is a notable second messenger that mediates signaling and leads to a multitude of adaptive physiological changes in response to cold and other stresses (Kudla *et al*, 2018). An intricate set of plant Ca^{2+} sensor proteins exhibit characteristic expression and subcellular localization profiles, as well as distinct Ca^{2+} affinities. Concomitantly, plants have complex signal-decoding machinery to process the wide range of Ca^{2+} signals into specific responses for stresses including temperature (Steinhorst & Kudla, 2013; Kudla *et al*, 2018). In rice, a recent report identified a potential thermosensor for high temperature stress. In this case, the heat stress-induced plasma membrane (PM)-localized E3 ligase Thermo-tolerance 3.1 (TT3.1) translocates from the PM to endosomes, where it ubiquitinates the chloroplast precursor protein TT3.2 for vacuolar degradation (Zhang *et al*, 2022). Another natural quantitative locus, TT2, regulates heat-triggered Ca^{2+} level and influences SENSING Ca^{2+} TRANSCRIPTION FACTOR 1 (SCT1)-calmodulin interaction in an Ca^{2+}-dependent manner, which ultimately affects wax biosynthesis and confers thermotolerance in rice (Kan *et al*, 2022). For the rice chilling response, a COLD1/RGA1 cold-sensing complex triggers Ca^{2+} signaling to elicit responses leading to cold tolerance (Ma *et al*, 2015). A cyclic nucleotide-gated channel, OsCNGC9, regulates cold-induced Ca^{2+} influx and cytoplasmic Ca^{2+} elevation in response to cold stress (Wang *et al*, 2021a). However, how Ca^{2+} signaling is triggered during cold stress has remained unclear.

1   Key Laboratory of Plant Molecular Physiology, Institute of Botany, Chinese Academy of Sciences, Beijing, China
2   University of Chinese Academy of Sciences, Beijing, China
3   Institut für Biologie und Biotechnologie der Pflanzen, Westfälische Wilhelms-Universität, Münster, Germany
4   Laboratory of Soft Matter Physics, Institute of Physics, Chinese Academy of Sciences, Beijing, China
5   State Key Laboratory of Plant Physiology and Biochemistry, College of Biological Sciences, China Agricultural University, Beijing, China
6   Innovation Academy for Seed Design, Chinese Academy of Sciences, Beijing, China
    *Corresponding author. Tel: +86 10 62836517; E-mail: chongk@ibcas.ac.cn
    †These authors contributed equally to this work.

In animal cells, the endoplasmic reticulum (ER) functions in a variety of cellular processes, including Ca^{2+} storage and release (Trewavas & Malho, 1998; Baumann & Walz, 2001; Groenendyk et al, 2004; Michalak et al, 2009). However, in plant cells, information on the Ca^{2+} storage properties of the ER is lacking. A previous study of ER Ca^{2+} dynamics in *Arabidopsis* demonstrated that the ER primarily functions as a Ca^{2+} buffer rather than a source, on the condition that various stimuli such as external ATP, L-Glu, and NaCl, triggered an elevation of $[Ca^{2+}]_{cyt}$, which was accompanied by ER Ca^{2+} accumulation (Bonza et al, 2013). Another study found that osmotic stress-induced increases in $[Ca^{2+}]_{cyt}$ are mainly attributable to extracellular Ca^{2+} influx, whereas increases in $[Ca^{2+}]_{nuc}$ are mediated by ER Ca^{2+} release, indicating that the ER is the source of nuclear Ca^{2+} elevation (Luo et al, 2020). Nevertheless, it remains controversial whether the ER contributes to the $[Ca^{2+}]_{cyt}$ increase upon osmotic stress in plant cells.

The ER-localized Ca^{2+}-binding protein calreticulin (CRT) is highly conserved and ubiquitous in different species, playing important roles in several processes such as Ca^{2+} signaling (Michalak et al, 1999). CRT has three distinct structural and functional domains: the N-domain, the P-domain (proline-rich central domain), and the C-domain (Nakamura et al, 2001; Persson et al, 2001; Wyatt et al, 2002; Jia et al, 2009). The N-domain is highly conserved and harbors a signal peptide sequence at its N-terminus. The P-domain has high-affinity and low-capacity Ca^{2+}-binding properties. The C-domain is highly acidic and contains many negatively charged residues that are responsible for Ca^{2+} binding. This domain binds to Ca^{2+} with high affinity and is involved in Ca^{2+} storage and modulating Ca^{2+} homeostasis (Nakamura et al, 2001; Jia et al, 2009). CRTs contain a typical K/HDEL ER-retention signal at the C-terminus, which mainly localize to the ER (Michalak et al, 1999), with some exceptions that plant CRTs have been reported outside the ER (Dedhar, 1994; Borisjuk et al, 1998; Baluska et al, 1999; Guo et al, 2003; Jia et al, 2008).

Calreticulin is an effective Ca^{2+} buffer with a potential role in transient Ca^{2+} storage and Ca^{2+} signaling. In animals, *CRT* overexpression increases cellular Ca^{2+} storage and alters the Ca^{2+} signaling response to external stimuli. Accordingly, *CRT*-deficient cells have reduced Ca^{2+} storage in the ER (Mery et al, 1996; Opas et al, 1996; Corbett & Michalak, 2000; Nakamura et al, 2001). In addition to the CRT1/2 group that functions in SA-dependent immune responses, plant cells have the plant-specific family member CRT3 (Jia et al, 2009; Qiu et al, 2012). CRT3 is a retention factor that interacts with proteins in the folding compartment and plays important roles in BR signaling and pollen tube germination in *Arabidopsis* (Jin et al, 2009; Li et al, 2011). In addition, the CRT3-SUN3/4/5-POD1 chaperone complex regulates the ER sorting of LRR receptor kinases to the plasma membrane (Xue et al, 2022). In plant cells, overexpression of *CRT* leads to greater Ca^{2+} release from the ER, resulting from enhanced Ca^{2+} binding capacity of CRT in the ER (Persson et al, 2001). However, it is still unclear how they functionally joint in the cold signal transduction, and how these proteins are connected to Ca^{2+} hemostasis and signal formation remains unknown.

Calcineurin B-like proteins (CBLs) and CBL-interacting protein kinases (CIPKs) play diverse roles in response to abiotic stresses (Halfter et al, 2000; Guo et al, 2001; Cheong et al, 2003; Xiang et al, 2007; Gu et al, 2008; Yang et al, 2008; Manik et al, 2015; Pandey et al, 2015; Thoday-Kennedy et al, 2015; Ma et al, 2020; Tang & Thompson, 2020; Wang et al, 2020; Plasencia et al, 2021). CIPKs have a kinase domain in the N-terminal region and a regulatory domain in the C-terminal region, which includes the NAF/FISL domain and the protein phosphatase interaction (PPI) domain. The NAF/FISL domain is auto-inhibitory and is also referred to as the CBL-binding domain. Upon binding to CBL, the CIPK kinase domain is released from the CIPK NAF/FISL domain, resulting in an active kinase conformation (Kim et al, 2000; Albrecht et al, 2001; Guo et al, 2001; Sanchez-Barrena et al, 2007; Chaves-Sanjuan et al, 2014; Sanyal et al, 2015; Tang et al, 2020). Most CBL proteins localize to the cell membrane, where they target CIPKs to form complexes. Accordingly, the core function of the CBL-CIPK network involves regulating membrane transport processes at the PM (Tang et al, 2020). In rice, OsCIPK7 plays a role in cold responses. A point mutation of OsCIPK7 led to a conformational change of the activation loop and enhanced its kinase activity, conferring increased chilling tolerance in rice (Zhang et al, 2019a). However, it is unclear what other Ca^{2+}-signaling-related proteins might contribute to cold signaling for establishing chilling tolerance.

In this study, we report that a rice calreticulin protein, OsCRT3, promotes chilling tolerance and mediates $[Ca^{2+}]_{cyt}$ elevation during cold-response signaling. We determined that OsCRT3 is an ER-localized protein and interacts with the protein kinase OsCIPK7. Cold-stress-induced conformational changes of OsCRT3 enhanced the OsCRT3-OsCIPK7 interaction, which boosted OsCIPK7 kinase activity. Further, the Ca^{2+} sensors OsCBL7 and OsCBL8 physically interacted with OsCIPK7 exclusively on the plasma membrane. Taken together, our data suggest that a cold-sensing mechanism and regulatory network involving OsCRT3 and OsCIPK7, as well as Ca^{2+} and its sensor OsCBL7/OsCBL8, are activated to promote chilling tolerance in rice.

Results

OsCRT3 is a positive regulator of chilling-stress response

ER-related Ca^{2+} processes play a crucial role in cold tolerance (Ma et al, 2015). CRTs are well-known ER-localized proteins with a K/HDEL signal peptide (Michalak et al, 1999). We investigated whether CRTs involved in cold signaling in rice. Interestingly, the expression of *OsCRT3* was specifically induced by cold treatment but not by drought and salt stress, compared with that of its homologs *OsCRT1* or *OsCRT2* (Fig EV1A and B). Rice *OsCRT3* is a single-copy gene located on chromosome 1, encoding a putative calreticulin orthologue. In the CRT3 family, most members were grouped into a branch that was parallel to CRT1/2 in the unrooted phylogenetic tree (Fig EV1C). To genetically analyze the function of *OsCRT3*, the *oscrt3-1* T-DNA insertion mutant was obtained (Jeon et al, 2000; Jeong et al, 2002). Sequencing data showed that the T-DNA was inserted at +110 bp from the ATG in the first exon of *OsCRT3* (Os01g67054). Quantitative PCR (qPCR) assays indicated that the intact *OsCRT3* transcript was undetectable in the *oscrt3-1* mutant, while a truncated transcript was present (Fig EV2). Thus, *oscrt3-1* is a loss-of-function mutant of *OsCRT3*.

To test the response of the *oscrt3-1* mutant to chilling stress, seedlings were exposed to 4°C for various durations. For up to 72 h

of chilling treatment, 85 % of the wild type grew well, but only 43 % of *oscrt3-1* seedlings survived. The difference in survival rate between wild type and the *oscrt3-1* mutant was more obvious over time during cold treatment (Fig 1A and D). By contrast, all lines overexpressing *OsCRT3* in the wild-type genetic background (Dongjin, DJ) showed significantly enhanced chilling-stress tolerance at the seedling stage (Fig 1B and E). Genetic complementation of *oscrt3-1* resulted in significantly enhanced chilling tolerance compared with the mutant (Fig 1C and F). The above results suggest that *OsCRT3* is required for chilling tolerance at the seedling stage in rice.

OsCRT3 is an ER-localized protein

OsCRT3 encodes a 446-amino acid (aa) protein with a predicted transmembrane domain (TMD) between amino acids 31 and 51. To dissect the subcellular localization of OsCRT3, mVenus was inserted downstream of the TMD (N$_{1-54}$:mVenus:OsCRT3, Fig 2A). The ER marker OFP-HDEL harbors a C-terminal HDEL ER-retention sequence and mainly localized in the ER lumen. The results of

transient assays in *N. benthamiana* epidermal cells showed that most of the N$_{1-54}$:mVenus:OsCRT3 colocalized with OFP-HDEL (Fig 2B–D). To further explore the localization of OsCRT3, N$_{1-54}$: mVenus:OsCRT3 was also co-expressed with the ER membrane marker AtCNX1-mCherry (Fig 2E–G). Colocalization analysis showed that N$_{1-54}$:mVenus:OsCRT3 exhibited a similar localization pattern to AtCNX1-mCherry. These data indicates that OsCRT3 localizes on the ER membrane and within the ER lumen. To investigate whether the N$_{1-54}$:mVenus:OsCRT3 construct retained proper OsCRT3 function in rice, complementation lines in the *oscrt3-1* background (N54-Com-L1) were used to detect cold-regulated gene expression under cold stress. Our results showed that both *DREB1A* and *DREB1B* were dramatically induced in N54-Com-L1 and DJ, to levels much higher than in *oscrt3-1* (Fig EV3A). This result demonstrates that the insertion of an mVenus tag behind the first 54 aa of OsCRT3 does not affect its function, as N$_{1-54}$:mVenus:OsCRT3 functioned properly in rice and rescued the *oscrt3-1* phenotype.

By contrast, when the mVenus tag was inserted before the TMD domain, N$_{1-33}$:mVenus:OsCRT3 localized to the cytosol and nucleus, indicating that insertion of mVenus at this site interfered with the
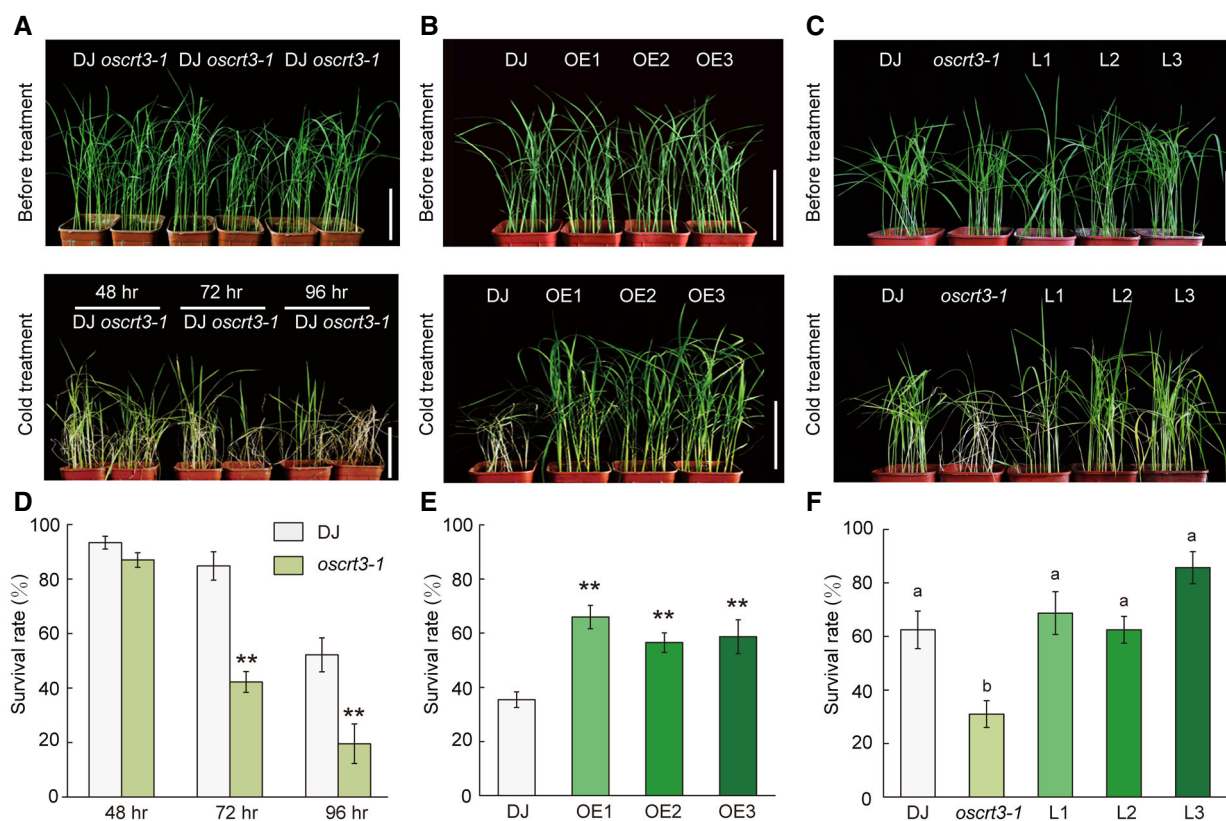

Figure 1. *OsCRT3* improves rice chilling tolerance at the seedling stage.

A Phenotype of wild-type (Dongjin) and *oscrt3-1* mutant seedlings incubated at 4°C for 48, 72, and 96 h. Bar: 5 cm.
B Phenotype of wild-type and *OsCRT3* transgenic overexpression lines (OE1, OE2, and OE3) seedlings incubated at 4°C for 100 h. Bar: 5 cm.
C Phenotype of wild-type, *oscrt3-1*, and *OsCRT3* complemented transgenic lines (L1, L2, and L3) seedlings incubated at 4°C for 96 h. Bar: 5 cm.
D, E Survival rates of cold-treated seedlings in (A) and (B). Data are means ± standard deviation (SD) of three biological replicates, with at least 15 plants per biological replicate. **$P < 0.01$, Student's *t*-test.
F Survival rates of cold-treated seedlings in (C). Data are means ± SD of three biological replicates, with at least 15 plants per biological replicate. Different letters represent statistically significant differences among the lines (Fisher's least significant difference test, $P < 0.05$).

natural localization of the peptide (Fig EV3B and C). Furthermore, when the ER-retention peptide (HDEL) at the C-terminus was mutated to AAAA in N_{1-54}:mVenus:OsCRT3, the fluorescent signal appeared in the cytosol, nucleus, chloroplast, and plasma membrane, instead of the ER (Fig EV3D and E). These results indicate that OsCRT3 localizes to the ER, and both its N-terminus and the C-terminus are essential for ER targeting.

OsCRT3 mediates cytoplasmic Ca^{2+} elevation for cold-response signaling

To examine the potential role of OsCRT3 in modulating Ca^{2+} fluxes or signal formation in response to cold, we monitored the Ca^{2+} concentration in the cytoplasm ($[Ca^{2+}]_{cyt}$) using cytosolic aequorin. Basal $[Ca^{2+}]_{cyt}$ levels in oscrt3-1 were lower than the wild type under normal temperature. $[Ca^{2+}]_{cyt}$ of wild-type Dongjin peaked rapidly after cold treatment and then gradually returned to normal levels. By contrast, there was a much smaller increase in oscrt3-1 $[Ca^{2+}]_{cyt}$ upon cold treatment, which was subsequently maintained at a nearly stable level under the same conditions. The genetically complemented line of the oscrt3-1 mutant (pOsCRT3) shared similar response patterns with wild type (Fig 3A and B).

A Yellow Cameleon (NES-YC3.6) assay was carried out to detect cytosolic Ca^{2+} signals upon cold stress. The signal ratio monitoring the spatiotemporal dynamics of Ca^{2+} fluxes in the cytoplasm showed that an obvious peak appeared after cold treatment in wild-type root cells. In contrast, the oscrt3-1 mutant showed a lower basal $[Ca^{2+}]_{cyt}$ level and a smaller peak of cold response in $[Ca^{2+}]_{cyt}$ compared with that of the wild type. The complemented line (pOsCRT3) almost rescued the reduced Ca^{2+} level in the oscrt3-1 background (Fig 3C). Together, these data suggest that OsCRT3 is an ER-resident protein that affects the cytoplasmic Ca^{2+} concentration in non-stimulated cells and modulates the release of Ca^{2+} to change cytoplasmic Ca^{2+} levels in response to cold temperature. These findings point to an underappreciated, crucial role of the ER as source compartment of Ca^{2+} for the formation of cold-induced cytoplasmic Ca^{2+} signals.

OsCRT3 interacts with OsCIPK7

Yeast two-hybrid assays using OsCRT3 as the bait identified 15 potential interactors (Appendix Table S1), including a putative calcineurin B-like protein-interacting protein kinase, OsCIPK7 (Os03g43440). Further interaction analyses revealed that the C-terminal domain of OsCRT3 mediates the interaction with the OsCIPK7 NAF/FISL domain, rather than its kinase domain (Fig 4A and B). The interaction between OsCRT3 and OsCIPK7 was confirmed by a pull-down assay. GST-OsCIPK7 was pulled down by MBP-OsCRT3 and not by the MBP control (Fig 4C). Taken together, these data indicate that OsCRT3 physically interacts with OsCIPK7.

qPCR analysis showed that OsCRT3 is constitutively expressed at various levels in all tissues tested (Fig EV4A), which is in agreement with the expression pattern of OsCIPK7 (Zhang et al, 2019a). OsCIPK7 expression was induced by cold, salt, and drought (Zhang et al, 2019a), while the expression of OsCRT3 was specifically induced by chilling treatment. Moreover, the expression patterns of OsCRT3 and OsCIPK7 in response to cold showed nearly overlapping curves (Fig EV1A, Zhang et al, 2019a). Further, OsCIPK7-GFP was

detected in the cytoplasm and nucleus and partially colocalized with the ER marker OFP-HDEL (Fig 4D–F), suggesting that OsCRT3 and OsCIPK7 both localize to the ER. Subcellular localization of OsCRT3 and OsCIPK7 was also characterized by immunoblot assays. N_{1-54}:mVenus:OsCRT3 was detected in the membrane fractions but not in the soluble fractions. In contrast, OsCIPK7-GFP was detected in both the membrane and soluble fractions. As controls, the membrane protein H^+-ATPase and ER protein Bip were detected in the membrane fractions, while GAPDH was only detected in the soluble fraction (Fig EV4B). The localization pattern of OsCIPK7 did not differ between wild type and oscrt3-1 (Fig EV4C), suggesting that OsCRT3 may not affect OsCIPK7 localization.

OsCIPK7 interacts with OsCBL7 and OsCBL8 on the plasma membrane

CBL-CIPK complexes are crucial in relaying plant responses to many environmental signals and in regulating ion fluxes (Batistič & Kudla, 2009; Kudla et al, 2018). Results of a yeast two-hybrid assay suggested that OsCIPK7 specifically interacts with the calcineurin B-like proteins OsCBL7 and OsCBL8 (Fig 5A). Subcellular localization analysis showed that OsCBL7-GFP and OsCBL8-GFP are localized at the PM after 2 days of expression in N. benthamiana leaves. However, a strong GFP signal could also be detected in the nucleus after 3 days of expression (Fig 5B). The interaction between OsCIPK7 and OsCBL7 or OsCBL8 was also verified by bimolecular fluorescence complementation (BiFC). Reconstituted YFP signal was detected at the PM (Fig 5C), suggesting that OsCIPK7 interacted with OsCBL7 and OsCBL8 specifically on the PM. These results indicate that OsCIPK7 may possess dual functions, depending on its interaction with either OsCBL7/OsCBL8 or OsCRT3, which would fulfill its functions at the PM or ER, respectively.

To test whether OsCRT3 affects the interaction of OsCBL7/OsCBL8 with OsCIPK7, a yeast three-hybrid (Y3H) assay was conducted, in which OsCRT3 was expressed under the Met25 promoter or GPD promoter. Expression of OsCRT3 under the Met25 promoter was repressed by 1 mM Met in the culture medium, while expression under the GPD promoter was normal. Expression of OsCRT3 fused with an HA tag was detected using an anti-HA antibody. The growth of yeast cells expressing OsCIPK7/OsCBL7-GPDOsCRT3 or OsCIPK7/OsCBL8-GPDOsCRT3 was slower than that of OsCIPK7/OsCBL7-MetOsCRT3 or OsCIPK7/OsCBL8-MetOsCRT3, indicating that OsCRT3 weakened the interaction between OsCIPK7 and OsCBL7/OsCBL8 in yeast cells (Fig 5D and E).

We conducted a Luciferase Complementation Imaging (LCI) assay, in which OsCBL7/OsCBL8-cluc and OsCIPK7-nluc were co-expressed with OsCRT3-mVenus or GFP. The intensity of luciferase fluorescence indicated the strength of the OsCBL7/OsCBL8-OsCIPK7 interaction. The results showed that expression of OsCRT3 reduced fluorescence intensity compared with that of the GFP control (Fig 5F). The expression of OsCIPK7-nluc, OsCBL7/OsCBL8-cluc, OsCRT3-mVenus and GFP was also validated by immunoblotting with anti-Luc, anti-cLuc and anti-GFP antibodies, respectively (Fig 5G). The pull-down assay also showed that OsCRT3 attenuated the interaction between OsCIPK7 and OsCBL7/OsCBL8. With increasing MBP-OsCRT3 levels, reduced amounts of MBP-OsCBL7 or MBP-OsCBL8 were pulled down by GST-OsCIPK7. However, no obvious difference was detected with increasing amounts of MBP,
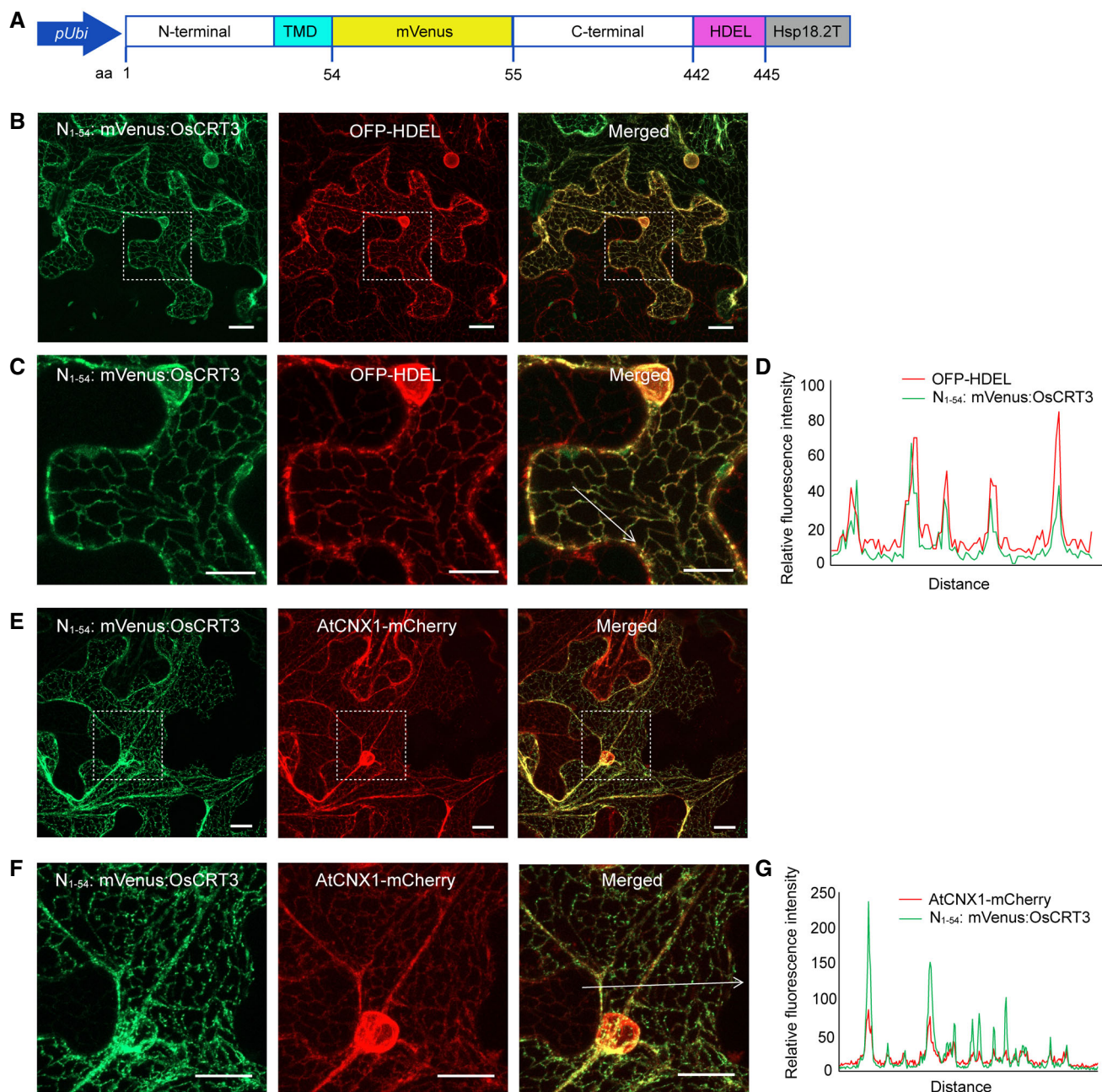
Figure 2. Subcellular localization of OsCRT3 in *N. benthamiana* leaves.

A   Schematic of the N$_{1-54}$:mVenus:OsCRT3 construct, with mVenus inserted downstream of the putative transmembrane domain (TMD), between aa 31 and 51 of OsCRT3. aa: amino acids.

B, C   Colocalization of N$_{1-54}$:mVenus:OsCRT3 with OFP-HDEL. OFP-HDEL is an ER lumen marker harboring a C-terminal HDEL ER-retention sequence. (C) shows a magnification of the box represented in (B). Bar: 20 μm.

D   Colocalization analyses along the white arrow in (C).

E, F   Colocalization of N$_{1-54}$:mVenus:OsCRT3 with the ER membrane marker AtCNX1-mCherry. (F) shows a magnification of the box represented in (E). Bar: 20 μm.

G   Colocalization analyses along the white arrow in (F).

which was used as a negative control (Fig 5H). Taken together, these results suggest that OsCIPK7 interacts with OsCBL7/OsCBL8 on the plasma membrane, and OsCRT3 attenuates the interaction between OsCIPK7 and OsCBL7/OsCBL8. Moreover, it also turns out that OsCRT3 and OsCBL7/8 bind the similar domain of OsCIPK7.

Cold treatment alters OsCRT3 conformation and enhances its interaction intensity with OsCIPK7

The secondary structure of OsCIPK7 shifts at different temperatures (Zhang *et al*, 2019a). Thus, to analyze whether cold stress alters the
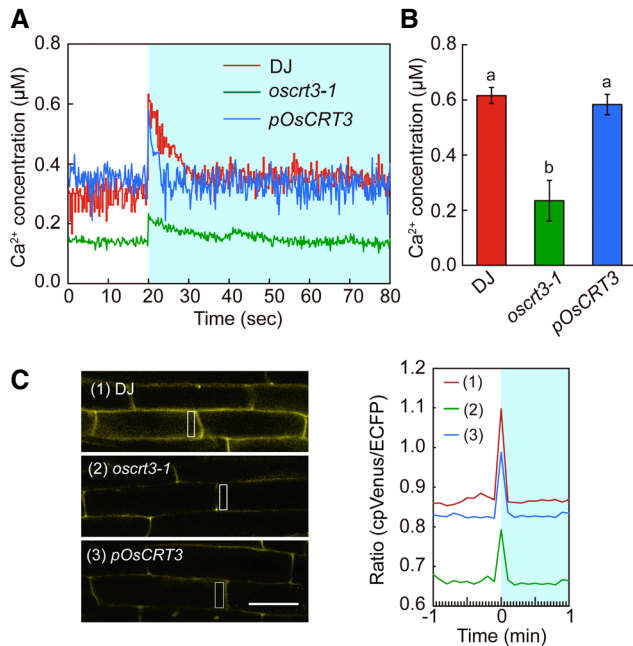
Figure 3. Ca²⁺ signaling upon cold shock in rice plants.

A Cytosolic free Ca²⁺ concentrations upon cold treatment of rice callus expressing aequorin in wild type (DJ), *oscrt3-1* mutant, and the *OsCRT3*-complemented transgenic lines (*pOsCRT3*). The blue background indicates cold treatment of the rice callus.

B Mean maximal Ca²⁺ influxes in (A). Values are expressed as means ± SD. At least 6 calli were used for each sample. Different letters represent statistically significantly differences among the lines (Fisher's least significant difference test, $P < 0.05$).

C Cold response of cytosolic free Ca²⁺ concentration in root cells expressing NES-YC3.6. Superimposition of representative normalized ratio variations for wild-type, *oscrt3-1*, and the complemented transgenic *pOsCRT3* root cells. The rectangle represents the regions of interest (ROIs) for the ratio measurements. The blue background indicates duration of cold treatment. Bar: 50 μm.

secondary structure of OsCRT3, Fourier-transform infrared (FTIR) spectroscopy assays were conducted (Li *et al*, 2020a, 2022). The secondary derivative spectra with the typical absorption peaks were denoted together with their assignments. The magnitude of negative peak in the second-derivative spectrum corresponds to the absorption intensity. When the temperature was shifted from 28°C to 5°C, there was an obvious increase of the β-sheet at 1,635 cm⁻¹, accompanied by a structural change from the hydrophilic α-helix at 1,650 cm⁻¹ to the hydrophobic α-helix at 1,652 cm⁻¹ (Fig 6A and B). These data showed that changes in OsCRT3 secondary structure occurred in response to cold treatment. RGA1 (G protein α unit), which plays a role in chilling tolerance in rice (Ma *et al*, 2015), was used as a negative control. The secondary structure of RGA1 did not show obvious changes under low temperature (Fig EV5A and B). To further support the results of our FTIR analysis, the three-dimensional structure of OsCRT3 was predicted with Alphafold2 (Jumper *et al*, 2021). Three main secondary structures exist in OsCRT3: random coil, α-helix, and β-sheet. The hydrophilic α-helix and hydrophobic α-helix are labeled, where the hydrophilic α-helix is extended (indicated with white arrows in Fig 6A), becoming more hydrophobic as temperature decreases. The approximate ratio of α-

helix: β-sheet: random coil in the predicted structure was 1:1.27:2.4, which is consistent with the FTIR structural analysis.

To investigate whether OsCRT3 conformational changes affect its interaction with OsCIPK7, the intensity of the OsCRT3-OsCIPK7 interaction was characterized by surface plasmon resonance (SPR) assay at 28 and 5°C. MBP-OsCRT3 proteins were captured on the CM5 chip immobilized with anti-MBP antibodies and tested for binding with gradient concentrations of OsCIPK7-C (from 2.5 to 40 μM at 28°C and from 0.625 to 10 μM at 5°C). The association rate constant (K_a) at 5°C was 684 ± 63 M⁻¹ s⁻¹, which was higher than 256 ± 96 M⁻¹ s⁻¹ at 28°C. The dissociation rate constant (K_d) at 5°C was lower than that at 28°C, which were 0.77 ± 0.19 × 10⁻³ s⁻¹ and 1.57 ± 0.43 × 10⁻³ s⁻¹, respectively. Kinetic values (K_D, K_d/K_a; equilibrium dissociation constant) decreased from 6.49 ± 1.48 μM at 28°C to 0.92 ± 0.21 μM at 5°C. Therefore, we observed enhanced binding affinity with a faster association rate and lower dissociation rate at 5°C compared with 28°C, indicating that cooling promoted tighter binding between OsCRT3 and OsCIPK7-C (Fig 6C and D). Taken together, our data suggest that cold stress leads to a conformational change of OsCRT3 and therefore enhances its interaction intensity with OsCIPK7.

The binding affinity of OsCIPK7-C and OsCBL8 exhibited a varied pattern as OsCRT3-OsCIPK7-C (Fig EV5C–E). Both the K_a and K_d at 5°C were lower than at 28°C, indicating that low temperature reduced the rate of association and dissociation, resulting in similar K_D values of 0.34 ± 0.04 μM and 0.39 ± 0.07 μM at 28 and 5°C, respectively. The K_D could not be measured under these OsCIPK7-C protein concentrations with 10 mM EGTA (Ca²⁺ chelator) in the running buffer, possibly suggesting that the OsCBL8-OsCIPK7 interaction is Ca²⁺-dependent.

OsCRT3 enhances the kinase activity of OsCIPK7

The kinase activation loop is important for CIPK activity in response to environmental stimuli (Guo *et al*, 2001; Yang *et al*, 2010). OsCIPK7 is a cold-activated protein kinase that plays a role in cold sensing in rice (Zhang *et al*, 2019a). An *in vitro* phosphorylation assay demonstrated that although OsCIPK7 showed autophosphorylation activity, it did not phosphorylate OsCRT3 or OsCBL7/OsCBL8 (Fig 7A and B). The NAF domain has an auto-inhibitory function in all CIPK-type kinases (Batistic & Kudla, 2009), and the Y2H assay indicated that OsCRT3 interacts with the OsCIPK7 NAF domain (Fig 4A and B). To test whether OsCRT3 affects the kinase activity of OsCIPK7, different amounts of OsCRT3 protein were incubated with OsCIPK7. With increasing OsCRT3 levels, there was enhanced OsCIPK7 kinase activity on the substrate myelin basic protein, along with greater OsCIPK7 autophosphorylation (Fig 7C). These data suggest that OsCRT3 physically interacts with OsCIPK7 to enhance its kinase activity in response to cold in rice.

Discussion

ER-localized OsCRT3 contributes to chilling tolerance in rice

As major chaperone proteins in the ER, CRTs play important roles in the storage of the rapidly exchanging pool of Ca²⁺ (Michalak *et al*, 2009). CRT3 is a plant-specific family member and differs from
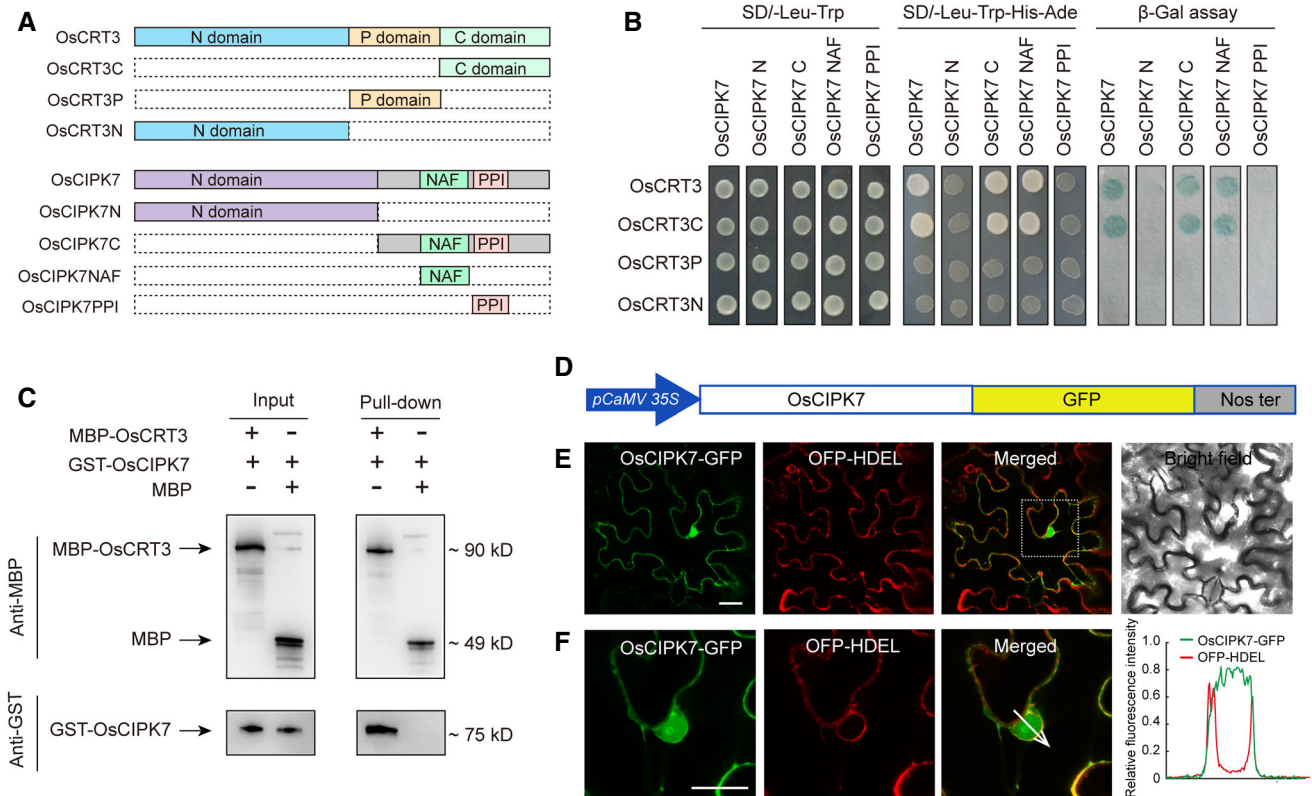
Figure 4. OsCRT3 interacts with OsCIPK7.

A Diagram of OsCRT3 and OsCIPK7 protein domains.
B Yeast two-hybrid analysis to test the OsCRT3–OsCIPK7 interaction. The interactions between OsCRT3, OsCRT3N, OsCRT3P or OsCRT3C with OsCIPK7, OsCIPK7N, OsCIPK7C, OsCIPK7NAF, or OsCIPK7PPI were verified.
C Pull-down assay of the interaction between OsCRT3 and OsCIPK7.
D Schematic of OsCIPK7-GFP construction.
E Localization of OsCIPK7-GFP in *N. benthamiana* leaf epidermal cells. OFP-HDEL was used as an ER marker. Bar: 20 μm.
F Magnification of the box represented in (E). Colocalization analyses along the white arrow are shown. Bar: 20 μm.

Source data are available online for this figure.

the CRT1/2 group that plays a role in SA-dependent immune responses (Fig EV1) (Jia *et al*, 2009; Qiu *et al*, 2012). In *Arabidopsis*, CRT3 functions as a key retention factor interacting with proteins in the folding compartment and is involved in BR signal transduction and pollen tube germination (Jin *et al*, 2009; Li *et al*, 2011). In addition, ER sorting of LRR receptor kinases to the PM is regulated by CRT3 together with its partners SUN3/4/5 and POD1 (Xue *et al*, 2022). However, how CRT regulates cold signaling remains to be

Figure 5. OsCIPK7 interacts with calcineurin B-like proteins OsCBL7/8.

A OsCIPK7 interacts with OsCBLs in a yeast two-hybrid system. Interactions were verified by growing the yeast on selective medium (SD/-Leu-Trp, SD/-Leu-Trp-His-Ade) and conducting β-galactosidase assays.
B Subcellular localization of OsCBL7 and OsCBL8 in *N. benthamiana* leaf epidermal cells. Pictures were taken after 2 and 3 days of expression. Bar: 50 μm.
C Bimolecular fluorescence complementation (BiFC) assay confirming the interaction between OsCBL7/8 and OsCIPK7 in *N. benthamiana* leaf epidermal cells. 19K was used as a negative control. Bar: 50 μm.
D Interactions between OsCIPK7 and OsCBL7 or OsCBL8 were attenuated by OsCRT3 in a yeast three-hybrid assay.
E Constructs and OsCRT3 protein expression level in (D).
F Luciferase Complementation Imaging assay (LCI) to detect the interaction between OsCIPK7-nluc and OsCBL7-cluc or OsCBL8-cluc, with co-expression of N_{1-54}:mVenus:OsCRT3 (mVenus-OsCRT3) or GFP, respectively. Quantification of luciferase activity was measured and shown. Values are mean ± SD. At least six leaves were used for each sample. *$P < 0.05$, Student's *t*-test. Experiments were repeated at least twice with similar results.
G Immunoblot confirming the expression of OsCIPK7, OsCBL7, OsCBL8, and OsCRT3 in (F) respectively.
H Pull-down assay showing that the interaction between OsCIPK7 and OsCBL7 or OsCBL8 was weakened with increasing amounts of OsCRT3. MBP was used as a negative control. Relative expression analysis was conducted using Image J software.

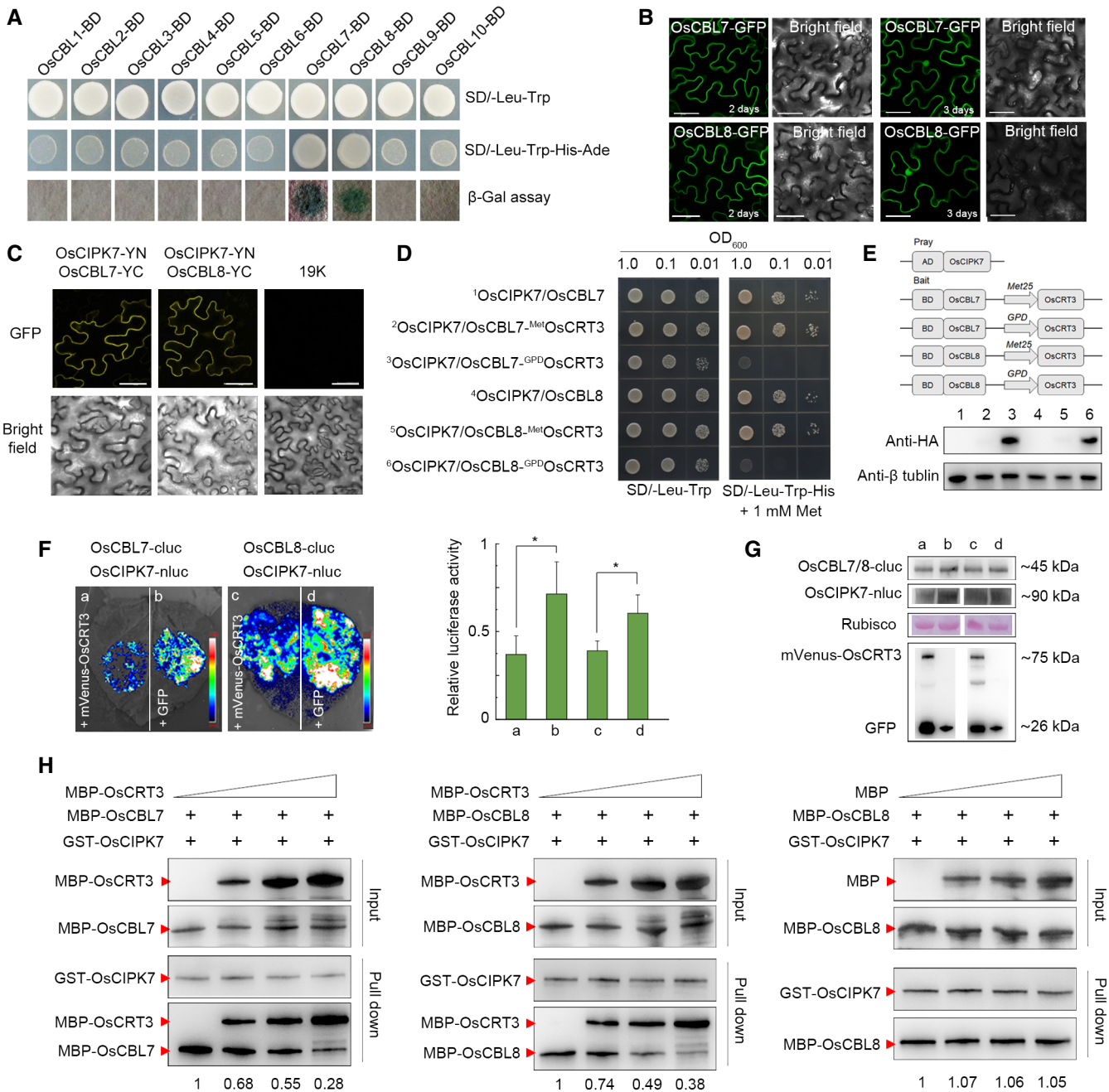Source data are available online for this figure.

Figure 5.

determined. Our results demonstrated that the plant-specific CRT member *OsCRT3* is highly induced by chilling stress and is genetically required for chilling tolerance in rice (Fig EV1). While the loss-of-function *oscrt3-1* mutant was more sensitive to chilling, its genetic complementation restored the wild-type phenotype. Conversely, *OsCRT3* overexpression lines exhibited increased tolerance to chilling (Fig 1).

CRTs possess a typical ER-retention signal (K/HDEL) at their C-terminus and mainly localize to the ER (Michalak *et al*, 1999). We generated the N_{1-54}:mVenus:OsCRT3 construct with the mVenus tag inserted downstream of the TMD to avoid artificial effects of the

mVenus tag. It was determined that OsCRT3 localized to the ER, and both the N-terminal and C-terminal regions of the protein are necessary for its correct localization (Figs 2 and EV3).

In animal cells, the ER is a Ca^{2+} store that plays a role in generating and shaping stimulus-induced cytosolic Ca^{2+} increases (Soboloff *et al*, 2012). In plant cells, however, it remains controversial whether the ER contributes to the $[Ca^{2+}]_{cyt}$ increase upon osmotic stress. A previous study in *Arabidopsis* suggested there is no evidence that the ER is a major source of Ca^{2+} release contributing to stimulus-induced increases in $[Ca^{2+}]_{cyt}$. The researchers proposed that the ER functions as "Ca^{2+} buffer" rather than a "Ca^{2+} source"
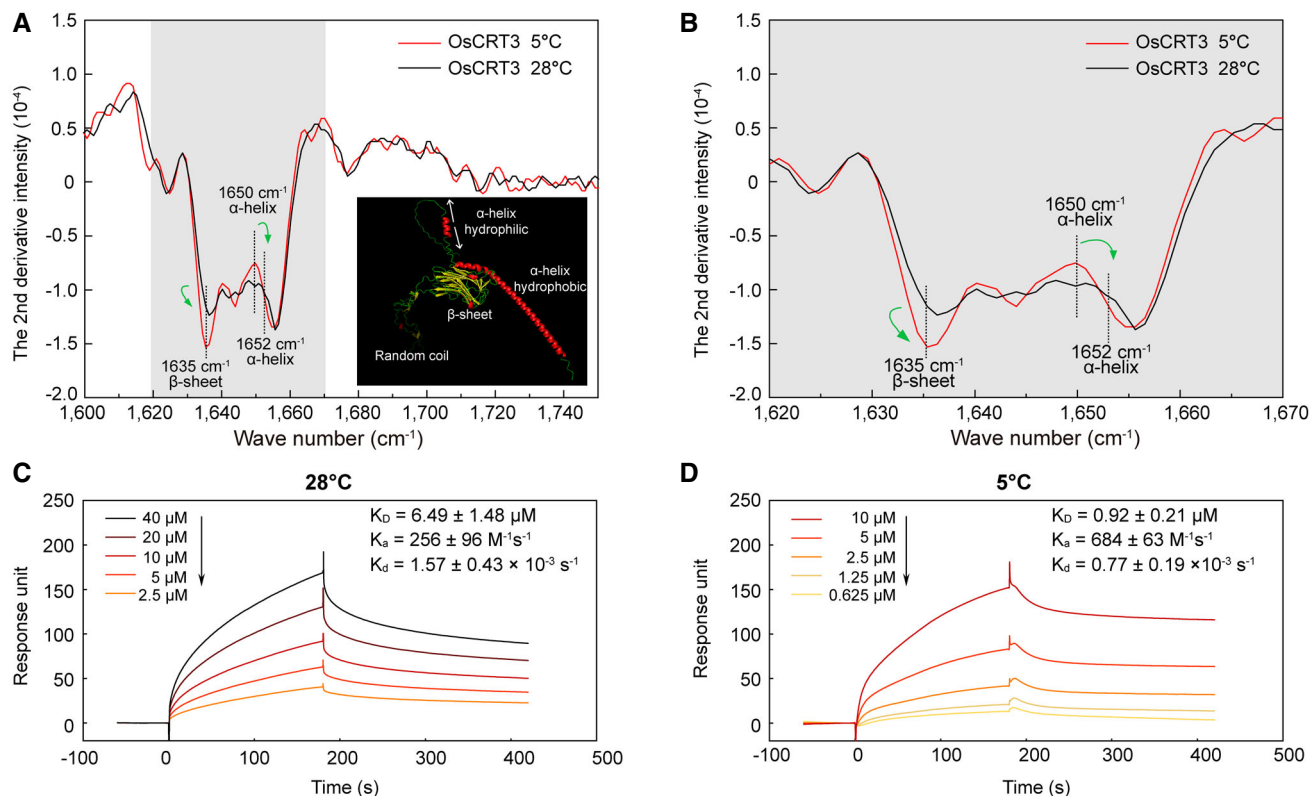
Figure 6. OsCRT3 exhibits conformational changes and enhanced binding affinity with OsCIPK7 upon cold stress.

A   Second-derivative infrared spectra of OsCRT3 at 5°C (red) and 28°C (black). Typical absorption peaks of secondary structures are denoted. 1,635 cm^{-1} (β-sheet), 1,640 cm^{-1} (random coil), 1,650 cm^{-1} (α-helix, hydrophilic), and 1,652 cm^{-1} (α-helix, hydrophobic). Predicted three-dimensional structure of OsCRT3 by Alphafold2 is shown in the lower right corner. Different secondary structures including random coil (green), α-helix (red), and β-sheet (yellow) are color-coded. The hydrophilic and hydrophobic α-helices are labeled. White arrows represent the hydrophilic α-helix becoming more hydrophobic with decreasing temperatures. The gray back-ground highlights part of the variated structure signals.

B   Magnified view of the gray highlighted area in (A), with the wave number ranging from 1,620 cm^{-1} to 1,670 cm^{-1}.

C, D   Interaction between OsCRT3 and OsCIPK7-C at different temperatures characterized by SPR. OsCRT3 proteins were captured on the CM5 chip immobilized with anti-MBP antibodies and tested for binding with gradient concentrations of OsCIPK7-C as indicated. HBS-P buffer containing 5 mM CaCl$_2$ was used as the running buffer. The K$_a$ (association rate constant), K$_d$ (dissociation rate constant), and K$_D$ (K$_d$/K$_a$, equilibrium dissociation constant) values were calculated using the Biacore T200 Evaluation software. Values are means ± SD from three technical replicates. At least two biological replicates were performed with similar results.

on the condition of different stimuli such as ATP, L-Glu, and NaCl (Bonza *et al*, 2013). However, recent research showed that increases in nuclear [Ca^{2+}] induced by external osmotic stimuli were caused by Ca^{2+} release from the ER (Luo *et al*, 2020). Our Ca^{2+} imaging data indicates that mutation of *OsCRT3* leads to decreased basal [Ca^{2+}]$_{cyt}$ and attenuates changes to [Ca^{2+}]$_{cyt}$ in response to chilling stress (Fig 3). Therefore, our data demonstrate that OsCRT3 is required for elevation of [Ca^{2+}]$_{cyt}$ upon cold stress. Our findings also support the notion that OsCRT3 is essential for an appropriate accumulation of Ca^{2+} in the ER that inversely affects the [Ca^{2+}]$_{cyt}$. The reduced "Ca^{2+} storage ability" of the ER in *oscrt3-1* results in a reduced [Ca^{2+}]$_{cyt}$ at resting conditions, indicative of essential storage and buffer functions of OsCRT3, and consequently the ER, under these circumstances. However, this reduced Ca^{2+} storage ability impairs the formation of transient cytoplasmic Ca^{2+} signals upon cold stimulation, revealing a "Ca^{2+} source function" of OsCRT3 and the ER under these conditions. On the other hand, ER-localized OsCRT3 (with OsCIPK7) may indirectly influence Ca^{2+} dynamics by affecting

other components such as Ca^{2+} channels. Taken together, ER-localized OsCRT3 mediates cytosolic Ca^{2+} increases essential for chilling tolerance in rice.

OsCRT3 conformational changes enhance binding to OsCIPK7 for sensing cold

The involvement of protein conformational changes in sensing ambient temperature to influence plant stress tolerance is a new concept. Our FTIR data suggested that OsCRT3 secondary structure undergoes changes in response to cold. Therefore, altered OsCRT3-OsCIPK7 conformation may sense cold to promote tolerance (Fig 6, Zhang *et al*, 2019a). The OsCRT3 C-terminal domain physically interacts with the NAF/FISL domain of OsCIPK7 (Fig 4). This interaction releases the NAF/FISL domain from the kinase domain to activate enzyme activity. Further, the kinase activity of OsCIPK7 was indeed enhanced with increasing amounts of OsCRT3 *in vitro* (Fig 7). Moreover, the interaction between OsCRT3 and OsCIPK7
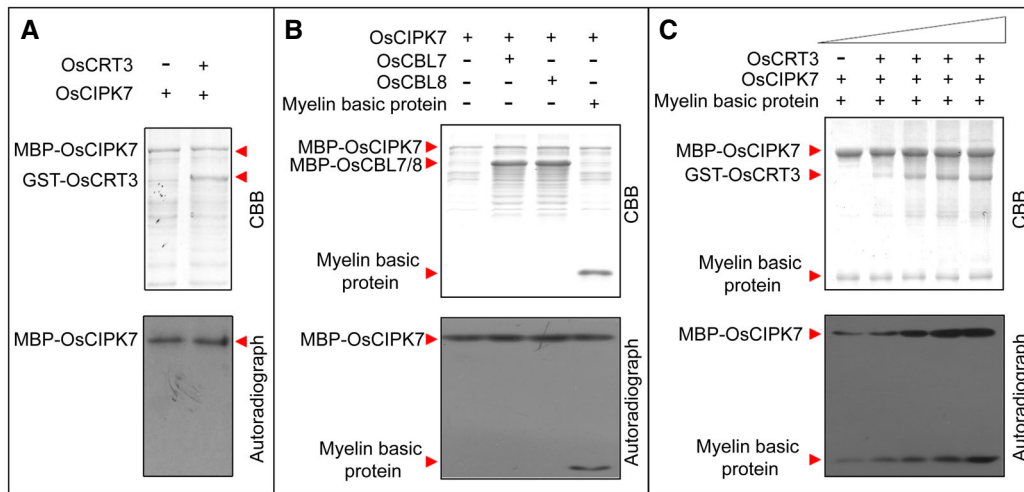
Figure 7. OsCRT3 enhances OsCIPK7 kinase activity.

A OsCIPK7 showed autophosphorylation activity but could not phosphorylate OsCRT3 *in vitro*. The loaded protein is indicated by red arrows. Autoradiograph of γ-^{32}P-labeled OsCIPK7 indicates autophosphorylation of OsCIPK7.

B OsCIPK7 did not phosphorylate OsCBL7 or OsCBL8 *in vitro*. Loaded proteins stained with Coomassie brilliant blue (CBB) are shown in the top panel and indicated by red arrows. Autoradiograph of γ-^{32}P-labeled myelin basic protein and OsCIPK7 are shown in the bottom panel.

C The kinase activity OsCIPK7 was enhanced with increasing concentrations of OsCRT3 protein. SDS-PAGE gel showing CBB-stained OsCRT3, myelin basic protein, and OsCIPK7 (top panel). γ-^{32}P-labeled myelin basic protein and OsCIPK7 substrate phosphorylation (bottom panel). The amount of OsCRT3 added was 0, 0.2, 0.4, 0.6, 0.8 μg in the SDS-PAGE gel lanes, respectively.

Source data are available online for this figure.

was strengthened upon cold treatment (Fig 6). These data suggest that altered secondary structures of OsCRT3-OsCIPK7 enhance their physical interaction, thereby activating OsCIPK7 kinase activity in response to cold. The OsCRT3-OsCIPK7 sensing complex may lead to activation of its downstream factors. Further studies are needed to unravel the molecular and mechanistic details of how cold-induced stimulation of OsCIPK7 activity at the ER translates into downstream responses for cold signaling and adaptation.

OsCRT3 conformational changes trigger the second messenger Ca^{2+} and induce enhanced binding to OsCIPK7 for sensing cold, which is supported by genetic evidence from the *oscrt3-1* mutant and overexpression lines (Fig 1). CBL is a Ca^{2+} sensor protein that binds Ca^{2+} and activates CIPK to trigger downstream reactions (Tang *et al*, 2020). In most cases, Ca^{2+} promotes the formation of the CIPK-CBL complex and activation of CIPK (Shi *et al*, 1999; Sanchez-Barrena *et al*, 2007), with some exceptions (Halfter *et al*, 2000; Guo *et al*, 2001; Ohta *et al*, 2003). *OsCBL7* and *OsCBL8* expression is induced by cold stress, and both OsCBLs have an N-myristoylation motif (MGXXXS/T) responsible for membrane targeting (Gu *et al*, 2008). Our data demonstrated that OsCBL7/OsCBL8 interacted with OsCIPK7 on the PM, and the interaction is Ca^{2+}-dependent (Figs 5 and EV5). Therefore, it is a downstream event for sensing Ca^{2+} elevation. It is hypothesized that the calcium released via OsCRT3 contributes to $[Ca^{2+}]_{cyt}$ elevation and may enhance OsCBL7/8-OsCIPK7 interaction on the PM.

The kinase activation loop is important for CIPK activity, and CIPKs function in plant responses to environmental stimuli (Batistic & Kudla, 2009). A mutant harboring a gain-of-function mutation within the *OsCIPK7* kinase domain exhibited increased Ca^{2+}

influx upon cold stress (Zhang *et al*, 2019a), indicating that OsCIPK7 may affect downstream proteins, such as Ca^{2+} channels, to indirectly regulate Ca^{2+} signaling. Although OsCIPK7 has autophosphorylation activity, it did not phosphorylate OsCRT3 or OsCBL7/OsCBL8 *in vitro* (Fig 7). It is proposed that OsCIPK7 transduces Ca^{2+} signals by phosphorylating downstream signaling components to respond to environmental stress. On the other hand, the data may indicate that OsCIPK7 has a dual function, interacting with OsCRT3 on the ER and OsCBL7/OsCBL8 on the PM. Moreover, OsCRT3 attenuates the interaction between OsCBL7/OsCBL8 and OsCIPK7, suggesting that OsCBL7 or OsCBL8 might also function in other cellular compartments besides the PM during a dynamic transient process, such as the ER. Further studies are needed to investigate the dual function of OsCIPK7 with these different interacting partners distributed among various cellular compartments.

Taken together, our study identified OsCRT3 as an ER-localized protein that affects both the basal and cold-responsive $[Ca^{2+}]_{cyt}$, suggesting that OsCRT3 and the ER may function as a Ca^{2+} source under cold stress. The cold-sensing OsCRT3-OsCIPK7 complex undergoes conformational changes under cold stress, leading to enhanced binding affinity and activation of OsCIPK7. Subsequently, OsCBL7/OsCBL8 sense the Ca^{2+} signals and specifically interact with OsCIPK7 on the plasma membrane (Fig 8). Based on our data from molecular and phenotypic analyses, we conclude that the rice cold-sensing mechanism involves conformational changes of OsCRT3-OsCIPK7 that ultimately promote chilling tolerance. Overall, our findings provide important insight for breeding strategies to improve chilling tolerance in rice.
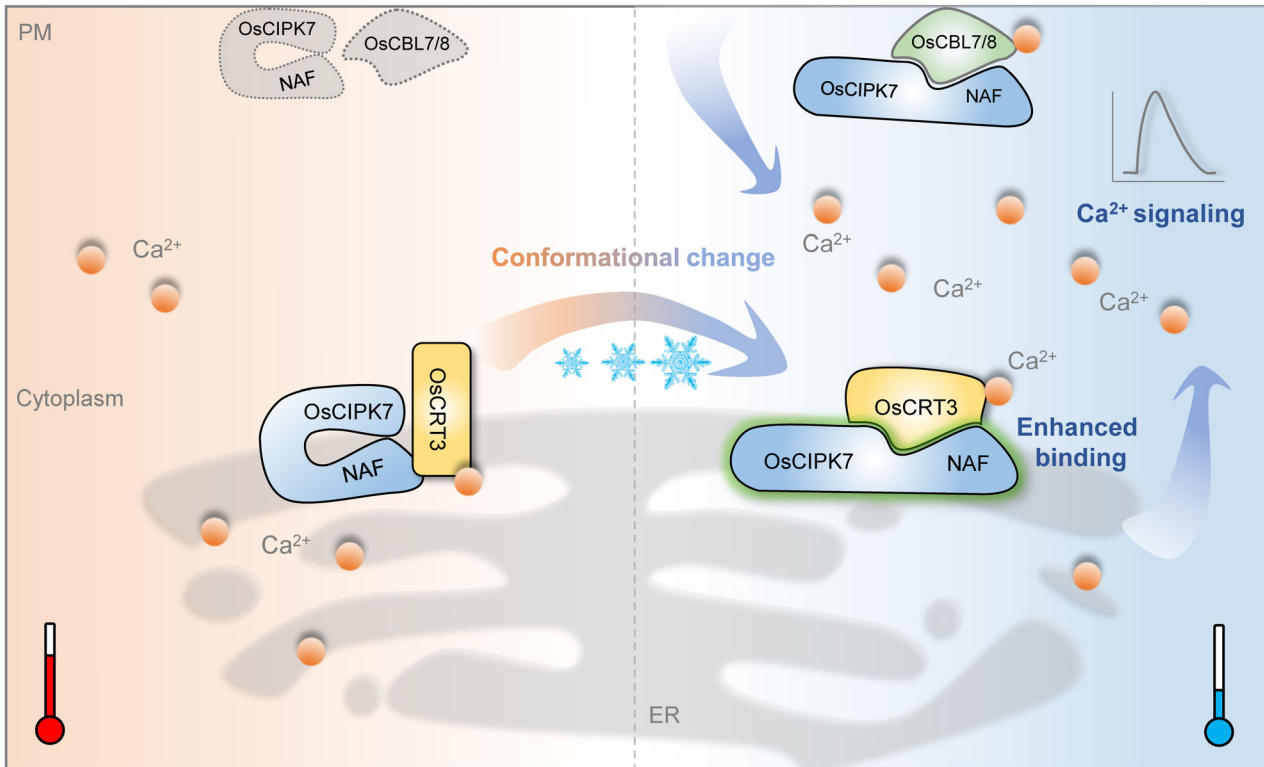
Figure 8. Proposed working model of OsCRT3–OsCIPK7–OsCBL7/8 in response to cold stress.

At normal temperatures, OsCRT3 slightly interacts with OsCIPK7. The auto-inhibitory status of the OsCIPK7 NAF/FISL domain represses its kinase activity. The cytosolic Ca^{2+} concentration ($[Ca^{2+}]_{cyt}$) is kept at a relatively low level. Upon chilling stress, cold signaling triggers OsCRT3 conformational changes to enhance its binding affinity with OsCIPK7, thereby boosting its kinase activity. Meanwhile, endoplasmic reticulum (ER)-localized OsCRT3 contributes to cold-induced $[Ca^{2+}]_{cyt}$ elevation, which is sensed by the Ca^{2+} sensor proteins OsCBL7/8 that specifically interact with OsCIPK7 on the plasma membrane (PM). This working model suggests a new regulatory network activated upon chilling stress in rice, composed of OsCRT3, OsCIPK7, along with Ca^{2+} and its sensors OsCBL7/OsCBL8.

Materials and Methods

Plant materials

The seeds of the *oscrt3-1* mutant (Dongjin genetic background) were obtained from the rice mutant database (http://signal.salk.edu/cgi-bin/RiceGE; Jeon *et al*, 2000; Jeong *et al*, 2002), Dongjin was used as the wild-type control. The *japonica* (*Oryza sativa*) cv Dongjin and Zhonghua10 (ZH10) were used for transformation. Transgenic plants derived from callus were defined as the T0 generation. Transgenic plants of the T1 and T2 generations were used for phenotypic analyses.

Plasmid construction and plant transformation

The full-length cDNAs of *OsCRT3* were amplified by PCR and ligated into *pUN1301* binary vectors for overexpression. The binary vectors were transformed into *Agrobacterium tumefaciens* strain EHA105, and then *Agrobacterium*-mediated transformation was conducted into rice calli (Hiei *et al*, 1994). The *OsCRT3* gene, including the promoter region and the coding region cloned from wild-type genomic DNA, was inserted into the vector *pCAMBIA1300* for genetic complementation tests. This construct was introduced into *oscrt3-1*

mutant plants by *Agrobacterium tumefaciens*-mediated transformation (Hiei *et al*, 1994). The independent homozygous transgenic lines were isolated and identified. The transgenic callus expressing aequorin was also used in determination of cytoplasmic Ca^{2+} concentration.

Chilling tolerance test of the mutant and transgenic plants

The chilling tolerance conditions were conducted as described (Ma *et al*, 2015; Zhang *et al*, 2019a). Seedlings with different genetic backgrounds were grown at a temperature of 28°C–30°C and 12 h/8 h day/night cycles in the greenhouse for 2 weeks, and then treated at 4°C for different time durations. After that, they were moved to the greenhouse for recovery for indicated time. The survival rate (percentage of live seedlings) was calculated after 7 days' recovery and used as an indicator of chilling tolerance.

Yeast two-hybrid assay

A yeast two-hybrid cDNA library of rice seedlings was constructed to identify proteins interacting with OsCRT3, using the Matchmaker system (Clontech). The open reading frame (ORF) of *OsCRT3* was amplified by PCR and then inserted into the GAL4

DNA binding-domain vector *pGBKT7* to act as bait. The rice cDNA library in the GAL4 activation domain vector *pGADT7* was constructed and screened according to the manufacturer's instructions (Clontech). The indicated combinations were transformed into yeast AH109 strain and grew on plates of medium-stringency medium in the absence of Trp and Leu and then tested on high-stringency medium SD/-Ade-His-Leu-Trp. Colonies showing a positive signal were subsequently examined for activation of the *lacZ* reporter gene.

For the verification of OsCRT3-OsCIPK7 interaction, different domains of OsCRT3 or OsCIPK7 were cloned into *pGBKT7* or *pGADT7* respectively, which was the same for OsCBL7/8-OsCIPK7 interaction. All the transformation colonies were grown on the SD/-Trp-Leu and SD/-Ade-His-Trp-Leu plates, followed by the examination of *LacZ* reporter gene with β-gal as a substrate.

Yeast three-hybrid assay

To detect the effect of OsCRT3 on the interaction of OsCIPK7 and OsCBL7 or OsCBL8, the yeast three-hybrid assay was conducted following the methods from (Ma *et al*, 2019; Li *et al*, 2020b). The *pBridge* vector was used with its original *MET25* promoter and modified *GPD* promoter. *GPD* promoter is a constitutive promoter while *MET25* promoter could be repressed with 1 mM methionine in the culture medium. The full-length *OsCBL7* or *OsCBL8* was cloned into the first multiple cloning site (MCS I) in the *pBridge* vector, and *OsCRT3* was cloned into the second cloning site MCS II with *MET25* promoter or *GPD* promoter respectively. *OsCIPK7* was cloned into *pGADT7* vector. The indicated combinations were transformed into yeast AH109 strain and growth on the SD medium plates lacking of Trp and Leu. Then the yeast transformants were cultured with SD (Trp-Leu-) overnight and adjusted OD_{600} to 1.0 before spotted on the plates. 10 μl of serial dillutions (1×, 10× and 100×) was dotted on SD plate (Trp-Leu-His) with 1 mM Met and then grew in 30°C for 3 days. To detect the expression of OsCRT3, the yeast cells were cultured with SD (Trp-Leu-His) with 1 mM Met overnight, and the cells were lysed with 1× SDS loading buffer and sonicated for 20 min. The expression of OsCRT3 with HA-tag was detected by Western blot using anti-HA antibody (abclonal, AE008). β-Tubulin was used as an internal reference using yeast anti-β-tubulin antibody (huaxingbio, HX20151).

Protein expression in *E. coli* and purification

For the proteins used in the pull-down and SPR assay, *OsCIPK7* or *OsCIPK7-C* terminus was cloned into the *pGEX4T-1* and *pGEX6p-1* vector respectively as a GST fusion protein. *OsCRT3*, *OsCBL7*, *OsCBL8* were cloned into the plasmid *pMAL-C2* as a fusion with maltose-binding protein (MBP). Then they were expressed in *E.coli* strain BL21(DE3) with 0.2 mM isopropyl β-D-thiogalactoside (IPTG) induced for 16 h at 16°C. The cells were collected with 5,000 *g*, 10 min at 4°C. And then the cells were lysed and sonicated by the lysis buffer (50 mM HEPES, 100 mM NaCl, pH 7.5). GST-tagged recombinant protein was purified by Glutathione Sepharose 4B (GE Healthcare, 17075605) and eluted by 20 mM GSH in lysis buffer, in which the pH was adjusted to 7.5. MBP-tagged recombinant proteins were purified by Amylose Resin (New England Biolabs, E8021) and eluted by 20 mM maltose in lysis buffer.

For the proteins used in phosphorylation assay, *OsCRT3* was cloned into the *pGEX4T-1* vector as a GST fusion protein. *OsCIPK7*, *OsCBL7*, and *OsCBL8* were cloned into the plasmid *pMAL-C2* as a fusion with maltose-binding protein (MBP). The expression and purification were conducted as described above.

For the proteins used in FTIR assay, *OsCRT3* or *RGA1* was cloned into the *pGEX6p-1* vector with a HRV 3C site between GST tag and target protein. The expression was performed according to the method above. The GST-tagged recombinant protein was also purified by Glutathione Sepharose 4B, and the beads were digested by PreScission Protease (Cytiva, 270843) on column at 4°C overnight. Then the cleaved protein was eluted by lysis buffer and concentrated with ultrafiltration tubes (Millipore) for the following procedures. The PreScission Protease was a GST-fused protein, which could be captured by GST beads and could not be eluted with the cleaved proteins. Purified proteins used in FTIR and SPR assays were shown by SDS-PAGE with CBB staining in Fig EV5F.

Pull-down assay

The purified proteins in the elution buffer were concentrated with ultrafiltration tubes (Millipore) and replaced by the lysis buffer to remove GSH or maltose. Then the purified proteins were used for pull-down assay (Wang *et al*, 2021b). For analysis the interaction between OsCIPK7 and OsCRT3, purified MBP-OsCRT3 or MBP was captured by Amylose Resin beads (New England Biolabs, E8021) at 4°C for 1 h and then incubated with GST-OsCIPK7 at 4°C overnight. For analysis the effect of OsCRT3 on OsCIPK7-OsCBL7/8 interactions, purified GST-OsCIPK7 was also captured by Glutathione Sepharose 4B beads at 4°C for 1 h and incubated with MBP-OsCBL7 or MBP-OsCBL8, along with increased gradient of MBP-OsCRT3 or MBP at 4°C overnight. The beads were washed by lysis buffer five times and then boiled in SDS-loading buffer for 10 min. Protein samples were separated by SDS-PAGE and then detected by Western blot analyses using anti-MBP monoclonal antibodies (New England Biolabs, E8032) and anti-GST antibody (EarthOx, E022210-01), respectively.

Total RNA isolation and quantitative PCR

Total RNA was extracted following the extraction kit (Invitrogen) according to the manufacturer's instructions. SYBR Premix Ex Taq (TAKARA) was used to perform quantitative PCR (qPCR) on 7500 real-time PCR system of Applied Biosystems. The thermal cycle was set as follows: 95°C for 3 min, then 40 cycles of 95°C for 30 s, 60°C for 30 s, and 72°C for 1 min. The rice *Actin1* (accession no. X16280) was used as an internal reference gene. The relative expression level was analyzed by the relative quantitative method (ΔCT) (Ma *et al*, 2015; Zhang *et al*, 2019a).

Protein extraction and immunoblot analyses

Leaves from tobacco were collected and ground in liquid nitrogen to a fine powder, and then total protein was extracted with ice-cold extraction buffer (20 mM Tris pH 8.0, 1 mM EDTA, 10% glycerin, 0.2% TritonX-100, 1 mM PMSF, and protease inhibitor cocktail [Roche]). The mixture was centrifuged at 10,000 *g* for 25 min at

4°C. Supernatant was filtered through four layers of Miracloth (Calbiochem). The filtered supernatant was centrifuged at 12,000 g for 30 min. Then the supernatant was transferred to a new ultracentrifuge tube (Beckman) and subsequently centrifuged at 100,000 g for 2 h at 4°C. The supernatant was collected, and the pellet was rinsed several times with cold extraction buffer. The pellet contained membrane proteins, and the supernatant contained soluble proteins. All the samples were mixed with SDS-PAGE loading buffer and boiled before gel fractionation. Immunodetection was performed using indicated antibodies with a secondary goat anti-rabbit or anti-mouse IgG horseradish peroxidase-conjugate antibody. Detection was performed using ECL-solution and imaged using illuminator. Western blot was conducted using GAPDH (Sigma, SAB2701826), H^+-ATPase (Agrisera, AS07260), Bip (Agrisera, AS09481), and GFP (abcam, ab6556) antibodies, respectively.

Subcellular localization

For subcellular localization analysis of OsCRT3 in *N. benthamiana* epidermal leaves, the N-terminal and C-terminal fragments of *OsCRT3* were PCR amplified and ligated into the vector *pGPTVII*, which contains the *AtUBI10* promoter and *AtHsp18.2* terminator. For the localization analysis of OsCIPK7 and OsCBL7/8 in *N. benthamiana* epidermal leaves, the coding region of these genes was cloned with *XbaI* and *KpnI* into *pBI121* vector respectively with a GFP tag in the C-terminus. All constructs were transformed into *Agrobacterium tumefaciens* strain GV3101 and then transformed into *N. benthamiana* leaves by *Agrobacterium*-mediated transformation (Waadt & Kudla, 2008).

For the localization analysis of OsCIPK7 in rice protoplast, the coding region of OsCIPK7 was cloned with *XbaI* and *KpnI* into pBI221 vector with a GFP tag in the C-terminus. Rice protoplasts were prepared according to the methods described in this paper (Ma *et al*, 2015). Images were obtained by confocal laser-scanning microscopy (Zeiss LSM 980). Colocalization analyses were conducted by ZEN 3.5 software.

Luciferase complementation imaging assay (LCI)

LCI assays were performed using a previously described protocol (Zhou *et al*, 2018). The full-length ORFs of *OsCBL7* or *OsCBL8* and *OsCIPK7* were cloned into *pCAMBIA1300*-cluc and *pCAMBIA1300*-nluc respectively. CBL7-cluc/OsCBL8-cluc, OsCIPK7-nluc plus N_{1-54}: mVenus: OsCRT3 or GFP were co-expressed in *N. benthamiana* epidermal leaves for 3 days. The luminescence images were captured using a CCD imaging system. The relative luciferase activity was measured and analyzed by Image J software. Western blot was conducted using anti-luciferase antibody (Sigma, L0159), anti-cluc antibody (sigma, L2164), and anti-GFP antibody (abcam, ab6556), respectively.

Fourier transform infrared (FTIR) assay

FTIR spectroscopy was performed as described (Li *et al*, 2020a, 2022). The OsCRT3 protein or RGA1 protein was freeze-dried through a vacuum at −10°C for lyophilization, and then the lyophilized proteins were dissolved in PBS buffer (50 mM K_2DPO_4/KD_2PO_4, pH7.4) containing 99.9% D_2O. FTIR absorption spectra at different temperatures were acquired on a spectrometer (VERTEX 70 V, Bruker Optics, Madison, WI, USA). A two-compartment CaF_2 sample cell with a 56-μm-thick Teflon spacer was used for the protein sample loading and reference. The measurements were conducted in a vacuum chamber equipped on FTIR spectrometer, and the temperature was controlled by a water circulator. Spectra were recorded at a resolution of 0.2 cm^{-1} in the region of 1,000–4,000 cm^{-1} where 60 scans were averaged. Second derivative analysis based on the absorption spectra exhibited a high spectral resolution, and the enhancement factor for a Gaussian type of lineshape was 1.88. The magnitude of negative peaks in the second derivative spectrum was corresponding to the absorption intensity, which was used for the absorption peak assignment in the FTIR spectrum.

Surface plasmon resonance (SPR) assays

Experiments were performed with a Biacore T200 optical biosensor instrument with CM5 chips (GE Healthcare, Biacore) at 28 or 5°C as indicated (Wang *et al*, 2016). All the proteins used in SPR were buffer-exchanged to HBS-P buffer (10 mM HEPES, pH 7.4, 150 mM NaCl, 0.005% surfactant P20) with 5 mM $CaCl_2$ or 10 mM EGTA, which was filtered through 0.22 μM micro membrane. MBP-OsCRT3 or MBP-OsCBL8 was captured by the immobilized MBP antibodies (New England Biolabs, E8038) on a CM5 sensor surface using standard amine-coupling procedures. MBP antibody in coupling buffer (10 mM sodium acetate, pH 5.0) was injected on the surface and remaining activated groups were blocked with 1 M ethanolamine, pH 8.5. MBP protein was captured in the control channel, which was used as a reference surface. The GST-OsCIPK7-C protein was serially diluted by HBS-P buffer to a serial of concentrations as indicated. The proteins were then flowed over the chip surface and the response units were measured. The true binding response was obtained by subtracting the value of control channel to eliminate the bulk effects. Results were interpreted using the BiaEvaluation software using 1:1 binding model (GE Healthcare).

Cytosolic aequorin Ca^{2+} concentration measurement

The calli expressing aequorin with different genetic backgrounds were incubated with 1 μM coelenterazine at 25°C for 16 h in darkness. Luminescence counts were recorded every 0.2 s in GLOMAX20/20 Luminometer (Promega, US) at room temperature. Then 300 μl of ice-cold water was injected into the cuvette after 20 s of counting, and the luminescence was continued to record for 1 min. Finally, 1 M $CaCl_2$ and 30% ethanol were added to discharge the remaining aequorin. Calculations of Ca^{2+} concentrations were performed as described (Ma *et al*, 2015).

FRET-based Ca^{2+} imaging

FRET-based Ca^{2+} imaging was performed on a Leica TCS SP5 system equipped with an inverted DMI6000 microscope stand, as described previously (Krebs *et al*, 2012; Ma *et al*, 2015). The rice seeds expressing Ca^{2+} biosensor NES-YC3.6 were germinated and grown at 28°C on 1/2 MS (Murashige and Skoog) medium plates for 4 days at 28°C. The Ca^{2+} imaging acquisition and analysis were performed as described (Ma *et al*, 2015).

BiFC assay

BiFC assays were performed as previously described (Waadt *et al*, 2008). The full-length of *OsCIPK7* and *OsCBL7* or *OsCBL8* were cloned into the *Xba*I and *Kpn*I sites of the *pSPYCE (M)* and *pSPYNE173* plasmids. Different combination of interactions was performed through *Agrobacterium*-mediated expression in *N. benthamiana* epidermal leaves, which was described above.

In vitro phosphorylation analysis

Phosphorylation analysis was performed as described (Zhang *et al*, 2019a). Appropriate amount of MBP-OsCIPK7 with GST-OsCRT3 or MBP-OsCBL7/8 was diluted in the kinase buffer (20 mM Tris–HCl, pH 8.0, 1 mM $CaCl_2$, 5 mM $MgCl_2$, 10 μM ATP, and 1 mM dithiothreitol). Myelin basic protein was used as a general substrate indicating the phosphorylation activity of protein kinase. 0.5 μl of γ-^{32}P-ATP (5 μCi) was added into the mixtures and then incubated at 30°C for 0.5 h. 6× SDS loading buffer was added to terminate the reaction and the samples were boiled at 95°C for 5 min. Samples were separated by 12% SDS-PAGE gels, following by staining with CBB (Coomassie brilliant blue). Then the gels were exposed to a phosphorus screen for more than 12 h, the autoradiograph of γ-^{32}P signals were acquired quantitatively using typhoon 9410 phosphor imager (Amersham Biosciences).

Data availability

This study includes no data deposited in external repositories.

Expanded View for this article is available online.

Author contributions

Xiaoyu Guo: Conceptualization; data curation; software; formal analysis; funding acquisition; investigation; visualization; methodology; writing – original draft. **Dajian Zhang:** Conceptualization; data curation; validation; investigation; visualization; methodology; writing – original draft. **Zhongliang Wang:** Formal analysis; investigation; methodology; writing – review and editing. **Shujuan Xu:** Investigation; methodology; writing – review and editing. **Oliver Batistič:** Validation; investigation; methodology; writing – review and editing. **Leonie Steinhorst:** Validation; investigation; methodology; writing – review and editing. **Hao Li:** Formal analysis; validation; investigation; methodology. **Yuxiang Weng:** Validation; investigation; methodology; writing – review and editing. **Dongtao Ren:** Validation; methodology. **Jörg Kudla:** Conceptualization; supervision; funding acquisition; methodology; writing – review and editing. **Yunxuan Xu:** Conceptualization; supervision; funding acquisition; writing – review and editing. **Kang Chong:** Conceptualization; supervision; funding acquisition; validation; writing – original draft; writing – review and editing.

References

Albrecht V, Ritz O, Linder S, Harter K, Kudla J (2001) The NAF domain defines a novel protein-protein interaction module conserved in Ca^{2+}-regulated kinases. *EMBO J* 20: 1051−1063

Baluska F, Samaj J, Napier R, Volkmann D (1999) Maize calreticulin localizes preferentially to plasmodesmata in root apex. *Plant J* 19: 481−488

Batistic O, Kudla J (2009) Plant calcineurin B-like proteins and their interacting protein kinases. *BBA-Mol Cell Res* 1793: 985−992

Baumann O, Walz B (2001) Endoplasmic reticulum of animal cells and its organization into structural and functional domains. *Int Rev Cytol* 205: 149−214

Bonza MC, Loro G, Behera S, Wong A, Kudla J, Costa A (2013) Analyses of Ca^{2+} accumulation and dynamics in the endoplasmic reticulum of *Arabidopsis* root cells using a genetically encoded Cameleon sensor. *Plant Physiol* 163: 1230−1241

Borisjuk N, Sitailo L, Adler K, Malysheva L, Tewes A, Borisjuk L, Manteuffel R (1998) Calreticulin expression in plant cells: developmental regulation, tissue specificity and intracellular distribution. *Planta* 206: 504−514

Chaves-Sanjuan A, Sanchez-Barrena MJ, Gonzalez-Rubio JM, Moreno M, Ragel P, Jimenez M, Pardo JM, Martinez-Ripoll M, Quintero FJ, Albert A (2014) Structural basis of the regulatory mechanism of the plant CIPK family of protein kinases controlling ion homeostasis and abiotic stress. *Proc Natl Acad Sci U S A* 111: E4532−E4541

Cheong YH, Kim KN, Pandey GK, Gupta R, Grant JJ, Luan S (2003) CBL1, a calcium sensor that differentially regulates salt, drought, and cold responses in *Arabidopsis*. *Plant Cell* 15: 1833−1845

Corbett EF, Michalak M (2000) Calcium, a signaling molecule in the endoplasmic reticulum? *Trends Biochem Sci* 25: 307−311

Dedhar S (1994) Novel functions for calreticulin: interaction with integrins and modulation of gene-expression. *Trends Biochem Sci* 19: 269−271

Groenendyk J, Lynch J, Michalak M (2004) Calreticulin, Ca^{2+}, and calcineurin - signaling from the endoplasmic reticulum. *Mol Cells* 17: 383−389

Gu ZM, Ma BJ, Jiang Y, Chen ZW, Su X, Zhang HS (2008) Expression analysis of the calcineurin B-like gene family in rice (*Oryza sativa* L.) under environmental stresses. *Gene* 415: 1−12

Guo Y, Halfter U, Ishitani M, Zhu JK (2001) Molecular characterization of functional domains in the protein kinase SOS2 that is required for plant salt tolerance. *Plant Cell* 13: 1383−1399

Guo L, Groenendyk J, Papp S, Dabrowska M, Knoblach B, Kay C, Parker JMR, Opas M, Michalak M (2003) Identification of an N-domain histidine essential for chaperone function in calreticulin. *J Biol Chem* 278: 50645−50653

Guo XY, Liu DF, Chong K (2018) Cold signaling in plants: insights into mechanisms and regulation. *J Integr Plant Biol* 60: 745−756

Halfter U, Ishitani M, Zhu JK (2000) The *Arabidopsis* SOS2 protein kinase physically interacts with and is activated by the calcium-binding protein SOS3. *Proc Natl Acad Sci U S A* 97: 3735−3740

Hiei Y, Ohta S, Komari T, Kumashiro T (1994) Efficient transformation of rice (*Oryza-Sativa* L) mediated by *Agrobacterium* and sequence-analysis of the boundaries of the T-DNA. *Plant J* 6: 271−282

Jeon JS, Lee S, Jung KH, Jun SH, Jeong DH, Lee J, Kim C, Jang S, Lee S, Yang K *et al* (2000) T-DNA insertional mutagenesis for functional genomics in rice. *Plant J* 22: 561−570

Jeong DH, An SY, Kang HG, Moon S, Han JJ, Park S, Lee HS, An KS, An GH (2002) T-DNA insertional mutagenesis for activation tagging in rice. *Plant Physiol* 130: 1636−1644

Jia XY, Xu CY, Jing RL, Li RZ, Mao XG, Wang JP, Chang XP (2008) Molecular cloning and characterization of wheat *calreticulin* (*CRT*) gene involved in drought-stressed responses. *J Exp Bot* 59: 739−751

Jia XY, He LH, Jing RL, Li RZ (2009) Calreticulin: conserved protein and diverse functions in plants. *Physiol Plant* 136: 127−138

Jin H, Hong Z, Su W, Li JM (2009) A plant-specific calreticulin is a key retention factor for a defective brassinosteroid receptor in the endoplasmic reticulum. *Proc Natl Acad Sci U S A* 106: 13612−13617

Jumper J, Evans R, Pritzel A, Green T, Figurnov M, Ronneberger O, Tunyasuvunakool K, Bates R, Zidek A, Potapenko A *et al* (2021) Highly accurate protein structure prediction with AlphaFold. *Nature* 596: 583−589

Kan Y, Mu X-R, Zhang H, Gao J, Shan JX, Ye WW, Lin HX (2022) TT2 controls rice thermotolerance through SCT1-dependent alteration of wax biosynthesis. *Nat Plants* 8: 53−67

Kim KN, Cheong YH, Gupta R, Luan S (2000) Interaction specificity of *Arabidopsis* calcineurin B-like calcium sensors and their target kinases. *Plant Physiol* 124: 1844−1853

Krebs M, Held K, Binder A, Hashimoto K, Den Herder G, Parniske M, Kudla J, Schumacher K (2012) FRET-based genetically encoded sensors allow high-resolution live cell imaging of Ca^{2+} dynamics. *Plant J* 69: 181−192

Kudla J, Becker D, Grill E, Hedrich R, Hippler M, Kummer U, Parniske M, Romeis T, Schumacher K (2018) Advances and current challenges in calcium signaling. *New Phytol* 218: 414−431

Li HJ, Xue Y, Jia DJ, Wang T, Shi DQ, Liu J, Cui F, Xie Q, Ye D, Yang WC (2011) POD1 regulates pollen tube guidance in response to micropylar female signaling and acts in early embryo patterning in *Arabidopsis*. *Plant Cell* 23: 3288−3302

Li H, Wang Y, Ye M, Li S, Li D, Ren H, Wang M, Du L, Li H, Veglia G *et al* (2020a) Dynamical and allosteric regulation of photoprotection in light harvesting complex II. *Sci China Chem* 63: 1121−1133

Li J, Zhou H, Zhang Y, Li Z, Yang Y, Guo Y (2020b) The GSK3-like kinase BIN2 is a molecular switch between the salt stress response and growth recovery in *Arabidopsis thaliana*. *Dev Cell* 55: 367−380

Li H, Yu Y, Ruan M, Jiao F, Chen H, Gao J, Weng Y, Bao Y (2022) The mechanism for thermal-enhanced chaperone-like activity of alpha-crystallin against UV irradiation-induced aggregation of gammaD-crystallin. *Biophys J* 121: 2233−2250

Luo J, Chen LL, Huang FF, Gao P, Zhao HP, Wang YD, Han SC (2020) Intraorganellar calcium imaging in *Arabidopsis* seedling roots using the GCaMP variants GCaMP6m and R-CEPIA1er. *J Plant Physiol* 246: 153127

Ma Y, Dai XY, Xu YY, Luo W, Zheng XM, Zeng DL, Pan YJ, Lin XL, Liu HH, Zhang DJ *et al* (2015) COLD1 confers chilling tolerance in rice. *Cell* 160: 1209−1221

Ma L, Ye J, Yang Y, Lin H, Yue L, Luo J, Long Y, Fu H, Liu X, Zhang Y *et al* (2019) The SOS2-SCaBP8 complex generates and fine-tunes an AtANN4-dependent calcium signature under salt stress. *Dev Cell* 48: 697−709

Ma X, Li QH, Yu YN, Qiao YM, ul Haq S, Gong ZH (2020) The CBL-CIPK pathway in plant response to stress signals. *Int J Mol Sci* 21: 5668

Manik SMN, Shi SJ, Mao JJ, Dong LH, Su YL, Wang Q, Liu HB (2015) The calcium sensor CBL-CIPK is involved in plant's response to abiotic stresses. *Int J Genomics* 2015: 493191

Mery L, Mesaeli N, Michalak M, Opas M, Lew DP, Krause KH (1996) Overexpression of *calreticulin* increases intracellular Ca^{2+} storage and decreases store-operated Ca^{2+} influx. *J Biol Chem* 271: 9332−9339

Michalak M, Corbett EF, Mesaeli N, Nakamura K, Opas M (1999) Calreticulin: one protein, one gene, many functions. *Biochem J* 344: 281−292

Michalak M, Groenendyk J, Szabo E, Gold LI, Opas M (2009) Calreticulin, a multi-process calcium-buffering chaperone of the endoplasmic reticulum. *Biochem J* 417: 651−666

Nakamura K, Zuppini A, Arnaudeau S, Lynch J, Ahsan I, Krause R, Papp S, De Smedt H, Parys JB, Muller-Esterl W *et al* (2001) Functional specialization of calreticulin domains. *J Cell Biol* 154: 961−972

Ohta M, Guo Y, Halfter U, Zhu JK (2003) A novel domain in the protein kinase SOS2 mediates interaction with the protein phosphatase 2C ABI2. *Proc Natl Acad Sci U S A* 100: 11771−11776

Opas M, SzewczenkoPawlikowski M, Jass GK, Mesaeli N, Michalak M (1996) Calreticulin modulates cell adhesiveness via regulation of vinculin expression. *J Cell Biol* 135: 1913−1923

Pandey GK, Kanwar P, Singh A, Steinhorst L, Pandey A, Yadav AK, Tokas I, Sanyal SK, Kim BG, Lee SC *et al* (2015) Calcineurin B-like protein-interacting protein kinase CIPK21 regulates osmotic and salt stress responses in *Arabidopsis*. *Plant Physiol* 169: 780−792

Persson S, Wyatt SE, Love J, Thompson WF, Robertson D, Boss WF (2001) The Ca^{2+} status of the endoplasmic reticulum is altered by induction of calreticulin expression in transgenic plants. *Plant Physiol* 126: 1092−1104

Plasencia FA, Estrada Y, Flores FB, Ortiz-Atienza A, Lozano R, Egea I (2021) The Ca^{2+} sensor calcineurin B-Like protein 10 in plants: emerging new crucial roles for plant abiotic stress tolerance. *Front Plant Sci* 11: 599944

Qiu YJ, Xi J, Du LQ, Roje S, Poovaiah BW (2012) A dual regulatory role of *Arabidopsis* calreticulin-2 in plant innate immunity. *Plant J* 69: 489−500

Sanchez-Barrena MJ, Fujii H, Angulo I, Martinez-Ripoll M, Zhu JK, Albert A (2007) The structure of the C-terminal domain of the protein kinase AtSOS2 bound to the calcium sensor AtSOS3. *Mol Cell* 26: 427−435

Sanyal SK, Pandey A, Pandey GK (2015) The CBL-CIPK signaling module in plants: a mechanistic perspective. *Physiol Plant* 155: 89−108

Shi JR, Kim KN, Ritz O, Albrecht V, Gupta R, Harter K, Luan S, Kudla J (1999) Novel protein kinases membraneciated with calcineurin B-like calcium sensors in *Arabidopsis*. *Plant Cell* 11: 2393−2405

Soboloff J, Rothberg BS, Madesh M, Gill DL (2012) STIM proteins: dynamic calcium signal transducers. *Nat Rev Mol Cell Biol* 13: 549−565

Steinhorst L, Kudla J (2013) Calcium and reactive oxygen species rule the waves of signaling. *Plant Physiol* 163: 471−485

Tang W, Thompson WA (2020) Role of the *Arabidopsis* calcineurin B-like protein-interacting protein kinase CIPK21 in plant cold stress tolerance. *Plant Biotechnol Rep* 14: 275−291

Tang RJ, Wang C, Li KL, Luan S (2020) The CBL-CIPK calcium signaling network: Unified paradigm from 20 years of discoveries. *Trends Plant Sci* 25: 604−617

Thoday-Kennedy EL, Jacobs AK, Roy SJ (2015) The role of the CBL-CIPK calcium signalling network in regulating ion transport in response to abiotic stress. *Plant Growth Regul* 76: 3−12

Trewavas AJ, Malho R (1998) Ca^{2+} signalling in plant cells: the big network! *Curr Opin Plant Biol* 1: 428−433

Waadt R, Kudla J (2008) In planta visualization of protein interactions using bimolecular fluorescence complementation (BiFC). *CSH Protoc* 2008: pdb.prot4995

Waadt R, Schmidt LK, Lohse M, Hashimoto K, Bock R, Kudla J (2008) Multicolor bimolecular fluorescence complementation reveals simultaneous formation of alternative CBL/CIPK complexes in planta. *Plant J* 56: 505−516

Wang H, Shi Y, Song J, Qi J, Lu G, Yan J, Gao GF (2016) Ebola viral glycoprotein bound to its endosomal receptor Niemann-Pick C1. *Cell* 164: 258−268

Wang L, Feng X, Yao LN, Ding CQ, Lei L, Hao XY, Li NN, Zeng JM, Yang YJ, Wang XC (2020) Characterization of CBL-CIPK signaling complexes and their involvement in cold response in tea plant. *Plant Physiol Biochem* 154: 195−203

Wang JC, Ren YL, Liu X, Luo S, Zhang X, Liu X, Lin QB, Zhu SS, Wan H, Yang Y *et al* (2021a) Transcriptional activation and phosphorylation of OsCNGC9 confer enhanced chilling tolerance in rice. *Mol Plant* 14: 315−329

Wang YJ, Gong Q, Wu YY, Huang F, Ismayil A, Zhang DF, Li HA, Gu HQ, Ludman M, Fatyol K *et al* (2021b) A calmodulin-binding transcription factor links calcium signaling to antiviral RNAi defense in plants. *Cell Host Microbe* 29: 1393−1406

Wyatt SE, Tsou PL, Robertson D (2002) Expression of the high capacity calcium-binding domain of calreticulin increases bioavailable calcium stores in plants. *Transgenic Res* 11: 1−10

Xiang Y, Huang YM, Xiong LZ (2007) Characterization of stress-responsive CIPK genes in rice for stress tolerance improvement. *Plant Physiol* 144: 1416−1428

Xue Y, Meng JG, Jia PF, Zhang ZR, Li HJ, Yang WC (2022) POD1-SUN-CRT3 chaperone complex guards the ER sorting of LRR receptor kinases in *Arabidopsis*. *Nat Commun* 13: 2703

Yang WQ, Kong ZS, Omo-Ikerodah E, Xu WY, Li Q, Xue YB (2008) Calcineurin B-like interacting protein kinase OsCIPK23 functions in pollination and drought stress responses in rice (*Oryza sativa* L.). *J Genet Genomics* 35: 531−543

Yang YQ, Qin YX, Xie CG, Zhao FY, Zhao JF, Liu DF, Chen SY, Fuglsang AT, Palmgren MG, Schumaker KS *et al* (2010) The *Arabidopsis* chaperone j3 regulates the plasma membrane H^+-ATPase through interaction with the PKS5 kinase. *Plant Cell* 22: 1313−1332

Zhang DJ, Guo XY, Xu YY, Li H, Ma L, Yao XF, Weng YX, Guo Y, Liu CM, Chong K (2019a) OsCIPK7 point-mutation leads to conformation and kinase-activity change for sensing cold response. *J Integr Plant Biol* 61: 1194−1200

Zhang JY, Li XM, Lin HX, Chong K (2019b) Crop improvement through temperature resilience. *Annu Rev Plant Biol* 70: 753−780

Zhang H, Zhou JF, Kan Y, Shan JX, Ye WW, Dong NQ, Guo T, Xiang YH, Yang YB, Li YC *et al* (2022) A genetic module at one locus in rice protects chloroplasts to enhance thermotolerance. *Science* 376: 1293−1300

Zhou Z, Bi G, Zhou JM (2018) Luciferase complementation assay for protein-protein interactions in plants. *Curr Protoc Plant Biol* 3: 42−50

Zhu JK (2016) Abiotic stress signaling and responses in plants. *Cell* 167: 313−324